

Microstructural evolution in Al–Cu–Fe quasicrystalline thin films

E.J. Widjaja*, L.D. Marks

Department of Materials Science and Engineering, Northwestern University, Cook Hall, 2225 North Campus Drive 2036, Evanston, IL 60208-3108, USA

Received 3 December 2002; received in revised form 17 May 2003; accepted 5 June 2003

Abstract

Transmission electron microscopy (TEM) was performed to study the microstructural evolution in Al–Cu–Fe quasicrystalline thin films. Thin films were grown by magnetron sputtering on sodium chloride crystals, which were subsequently dissolved in water to acquire free-standing films. Studies were conducted on the as-deposited sample, and samples that were annealed at 400 °C in Argon and 500 °C in air. Nanocrystalline films were found in the as-deposited sample. When annealed at 400 °C the films changed to a metastable crystalline cubic β -phase as the dominant phase with secondary phases (θ - and ω -phases), which appear as small islands and precipitates on the surfaces, in the matrices and at grain boundaries, with specific orientations with respect to the cubic β -phase. The metastable phase transformed into the icosahedral ψ -phase plus residual Al-rich material (including λ -phase) upon further annealing at 500 °C. TEM imaging combined with electron diffraction revealed various features associated with the phase evolution in the crystalline–quasicrystalline phase transformation. Some grains in the film functioned as sacrificial grains allowing others to grow into icosahedral phases. Elements near the boundary of the sacrificial grains diffused to form the ψ -phase, resulting in fragments in the center of the grain. The roles of the sacrificial grains and elements diffusions, and the phase transformation mechanism are discussed. Additionally, the oxide layer of the film was an amorphous aluminum oxide that exhibited poor adhesion to the quasicrystalline films.

© 2003 Elsevier B.V. All rights reserved.

Keywords: Quasicrystalline thin films; Microstructural evolution; Transmission electron microscopy (TEM); Al–Cu–Fe

1. Introduction

Quasi-periodic crystals, commonly referred to as quasicrystals, are intriguing structures, which demonstrate properties that are very different from conventional metallic materials. They show a long-range order with traditionally forbidden rotational symmetries such as five-fold and 10-fold rotation axes. Even though quasicrystals are mostly metallic alloys, they exhibit high hardness and stiffness with low electrical and thermal conductivities. The coefficient of friction and surface energy of the quasicrystalline materials are also very low. These attractive properties of quasicrystalline materials have been exploited in the industry for thin coating applications of conventional crystalline materials [1,2]. At present, in addition to the second phase precipitates, thin films/coatings are the only viable forms for prac-

tical applications since bulk quasicrystals are extremely brittle. Reviews of the properties and applications of quasicrystalline materials can be found elsewhere [1,3–6].

The Al–Cu–Fe system was first studied by Tsai [7] because of its low friction property. The phase diagram, microstructure and phase transformations in Al–Cu–Fe bulk quasicrystals have been widely studied [8–11]. Relatively little research has been conducted along these lines for Al–Cu–Fe quasicrystalline thin films; the majority of the work has emphasized the deposition method [12–18], annealing process [19], properties measurement [12,19–22] and oxidation behavior [23], plus some work studying the structural evolution of Al–Cu–Fe quasicrystalline thin films using X-ray diffraction (XRD) [24,25].

In most studies of Al–Cu–Fe films, only XRD was used to characterize the phases, however, the Al–Cu–Fe phase diagram with the crystalline phases, the rhombohedral R-phase, the orthorhombic O-phase, pentagonal

*Corresponding author. Tel.: +1-847-4917809; fax: +1-847-4917820.

E-mail address: e-widjaja@northwestern.edu (E.J. Widjaja).

phases, modulated and perfect icosahedral phases is very complex [8–11,26]. These phases show only small differences in their XRD patterns [11,26]. These small differences are further complicated in thin films due to finite grain size effect and other defects. In addition, XRD does not offer detailed information on the local microstructure.

Transmission electron microscopy (TEM) is a powerful tool to study the structure and morphology of quasicrystal. Although TEM has been used to evaluate the microstructural evolution in thin films of various quasicrystal systems, much of the work focused on thin films that were prepared by depositing layers of different pure elements, such as high temperature sequential deposition of Al and Mn [27], sputtering deposition to form multilayers of Al and Cr [28] and successive

electron-beam evaporation of multilayers of Al and Co [29].

While there are studies using TEM to study Al–Cu–Fe quasicrystalline thin films (for example [30,31]), there has been little emphasis on the microstructural evolution. The objective of this article is to present TEM studies of Al–Cu–Fe quasicrystalline thin films prepared by single-target magnetron sputtering and the evolution of their microstructure during the phase transformation on heating.

2. Experimental details

Thin films of Al–Cu–Fe were grown on cleaved sodium chloride substrates in a magnetron sputtering chamber with a base pressure of 3×10^{-8} Torr. Deposi-

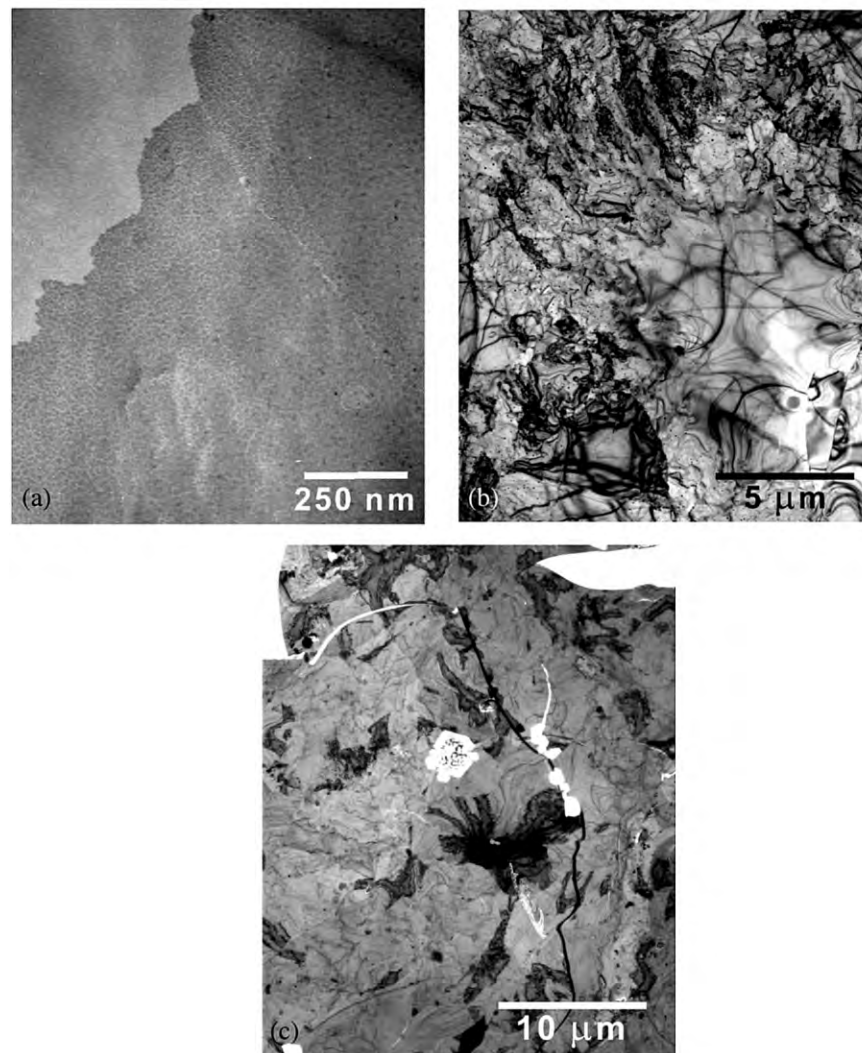


Fig. 1. TEM bright field images of Al–Cu–Fe thin films in: (a) the as-deposited condition; (b) the sample annealed at 400 °C in Ar; (c) the sample annealed at 500 °C in air.

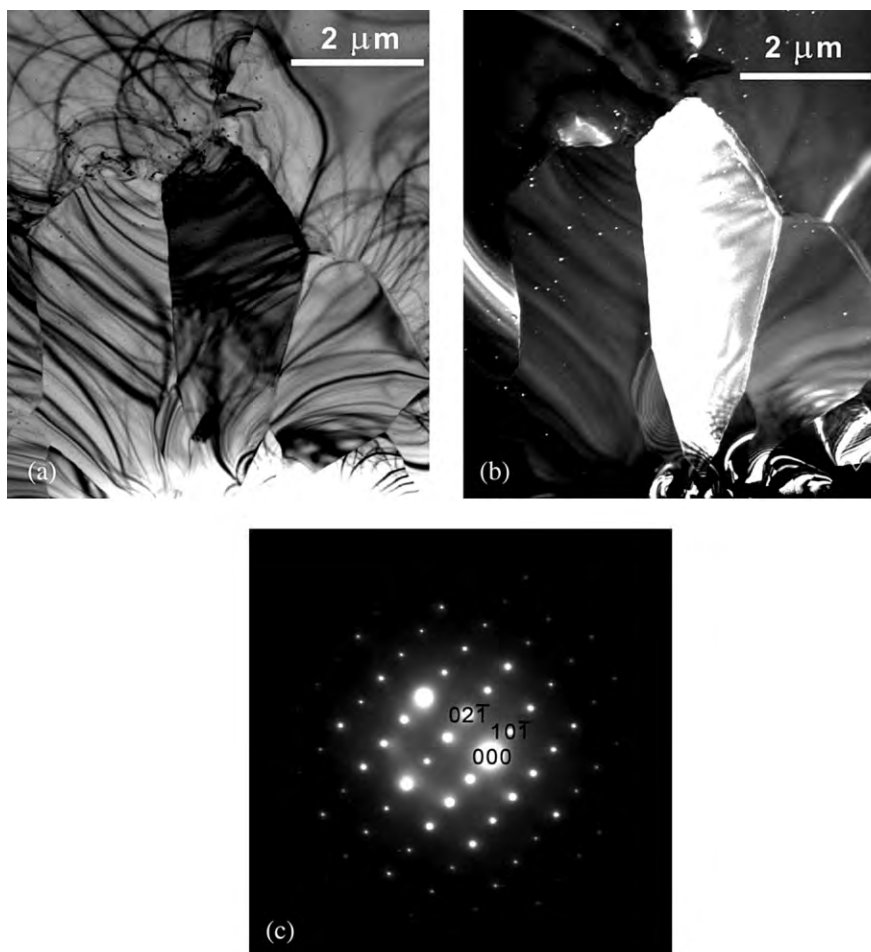


Fig. 2. Observations made in thin film annealed at 400 °C in Ar: (a) TEM bright field image; (b) TEM dark field image; and (c) the electron diffraction pattern showing 212 zone axis of cubic crystalline β -phase.

tions were carried out at 2.8 mTorr Argon (99.998% purity), 150 W and at room temperature without a substrate bias. The target was a metal alloy made through vacuum arc melting. After the deposition process, the samples were cleaved into two parts. One part was kept in the as-deposited state while the other sample was annealed in a furnace (at atmospheric pressure) with a continuous flow of Argon at 400 °C for 4 h. The annealed sample was then cut into two sections, and one was annealed further at 500 °C in air for an additional 4 h.

The sodium chloride substrates were subsequently removed by dissolving in water to acquire free-standing thin films of thickness approximately 150–200 nm. These thin films were then suspended on Mo hole-grids and studied using a Hitachi H-8100 TEM. The relative metallic compositions were determined from energy dispersive X-ray (EDX) spectroscopy, calibrated using single crystal icosahedral $\text{Al}_{63}\text{Cu}_{25}\text{Fe}_{12}$ as the standard. To detect the phase transformations, differential scanning

calorimetric (DSC) studies were carried out from room temperature to 600 °C at a heating rate of 5 °C/min.

3. Results and discussion

Fig. 1a–c show TEM bright field images of films in the as-deposited condition and after the aforementioned annealing treatments. The as-deposited sample (Fig. 1a) shows a nanocrystalline structure with a grain size < 10 nm. This structure was attributed to a combination of a rapid quenching effect and a small increase of the substrate temperature due to atom bombardments during deposition. The sample annealed at 400 °C (Fig. 1b) showed mostly a continuous film while the sample treated at 500 °C (Fig. 1c) exhibited some level of discontinuity across the thin film.

While there are few reports that claim the structure of the room-temperature as-deposited samples to be amorphous [31,32], this is almost strictly correct only when the substrate is cooled (e.g. to liquid nitrogen [33]

or liquid helium [34] temperatures) or when substrate heating due to atomic bombardment can be prevented (e.g. the growth of very thin films [35]). Production of

amorphous films requires very high deposition rates and low-substrate deposition; the latter immobilizes or freezes adatoms on the substrate where they impinge and

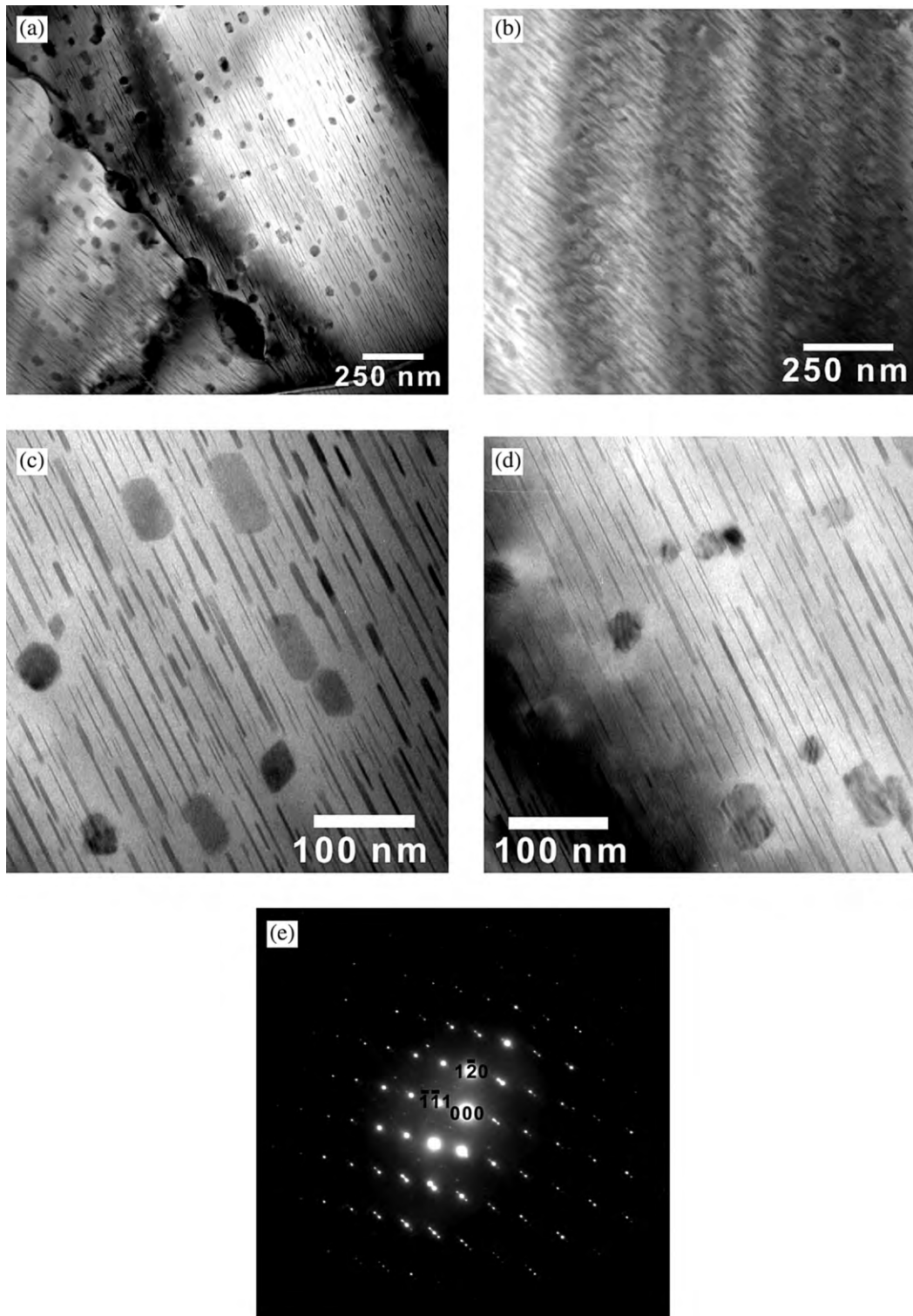


Fig. 3. (a–b) TEM bright field images of films annealed at 400 °C in Ar showing small precipitates and islands on larger cubic β -grains and larger precipitates at the grain boundaries; (c–d) islands on the β -phase matrix and; (e) diffraction pattern of (a) near 213 zone axis of cubic crystalline β -phase.

prevents them from diffusing and seeking out equilibrium lattice sites [36]. Due to the small grain sizes, nano-scale crystalline phases are generally indistinguishable from amorphous phase in XRD studies; however, they are easily observable in TEM imaging.

The sample annealed at 400 °C in Ar was composed of crystalline grains with an average grain size of a few microns, as shown in Fig. 2a–c. Note that the average composition of the film in the sample annealed at 400 °C in Ar was $\text{Al}_{64\pm3}\text{Cu}_{23\pm2}\text{Fe}_{13\pm1}$. Upon annealing at 400 °C, the film formed large grains of intermetallic phases, demonstrating conventional grain growth driven by the reduction of grain boundary energy. No phase transformation to the quasicrystalline phase was observed. This finding was confirmed by DSC, which showed an exothermic peak at 440 ± 15 °C.

The structure of the intermetallics is the CsCl cubic β -phase, $\text{Al}(\text{Fe}, \text{Cu})$ with a lattice parameter of 0.294 nm. A diffraction pattern along the $\langle 212 \rangle$ zone axis is shown in Fig. 2c. This cubic structure is similar to the β -phase in the bulk phase diagram [11] that extends over a large range of composition. A similar structure also appeared on the surface of a single grain icosahedral Al–Cu–Fe alloy upon ion bombardment [37–39]; this was attributed to the preferential sputtering of aluminum from the surface.

The crystalline cubic β -phase in the 400 °C annealed sample is a metastable phase at this composition and temperature, however, there may be other metastable crystalline phases. In addition, to the micron sized cubic β -phase grains, smaller grains of sizes less than 50 nm appear in the form of precipitates or islands at the surface, while larger grains of approximately 100–200 nm were found at grain boundaries, as shown in Fig. 3a.

In addition to the majority cubic β -phase, Chien and Lu [33] reported the existence of a second phase in their sample upon annealing at 450 °C based on their XRD results, but were uncertain whether the second phase was cubic β -crystals with small grain sizes or amorphous. It needs to be noted that their film was deposited at liquid nitrogen temperature to try and produce an initial amorphous phase. However, it is unlikely that the original amorphous phase will remain after the annealing treatment.

The secondary phases in our sample are crystalline with small grains that appear as precipitates and islands—in the matrices, on the surface and at grain boundaries. Fig. 3b is a TEM bright field image of a grain showing needle precipitates along with islands; this image is equivalent to tilting the grain in Fig. 3a. Combining these two images, it appears that the precipitates assume the shape of platelets and are highly textured with the matrices. The islands on the surface can be either textured with specific facets and orientations with respect to the matrix (Fig. 3c) or not (Fig.

3d). Moire fringes are observed for islands in Fig. 3d, due to superposition of periodic lattices with angle orientations.

The β -phase in the bulk phase diagram has the composition of $\text{Al}_{50}\text{Fe}_{50-x}\text{Cu}_x$ (extends from AlFe up to 40% atomic percentage Cu) [40]. Although the average composition of the grains, $\text{Al}_{64\pm3}\text{Cu}_{23\pm2}\text{Fe}_{13\pm1}$, is closer to the ω -phase (tetragonal $\text{Al}_7\text{Cu}_2\text{Fe}$ with $a=0.634$ nm and $c=1.487$ nm), the larger grained crystalline phase is the cubic β -phase. Nevertheless, the true composition of the β -phase in the films may be less than the average composition due to contribution from the secondary phases. It is likely that the secondary phases are the θ -phase (tetragonal Al_2Cu with $a=0.6063$ nm and $c=0.4872$ nm) and/or the ω -phase. Both the θ - and ω -phases are richer in aluminum than the β -phase, allowing the reduction of aluminum content in the matrices, hence, gives more stability to the β -phase. The θ -phase can be incorporated into the β -phase matrix coherently with relatively small strains, $\varepsilon_x = \varepsilon_y = (2a_\beta - a_\theta)/2a_\beta = 3.1\%$ and $\varepsilon_z = (5a_\beta - 3c_\theta)/5a_\beta = 1.2\%$.

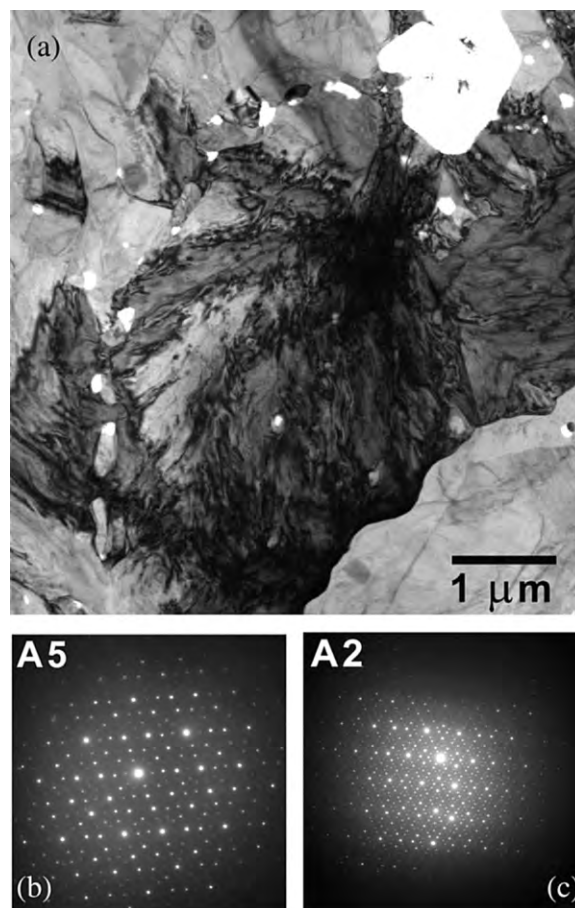


Fig. 4. (a) Bright field image of an icosahedral grain oriented along a zone axis; (b) Electron diffraction pattern of icosahedral phase showing five-fold symmetry; and (c) Electron diffraction pattern of icosahedral phase showing two-fold symmetry.

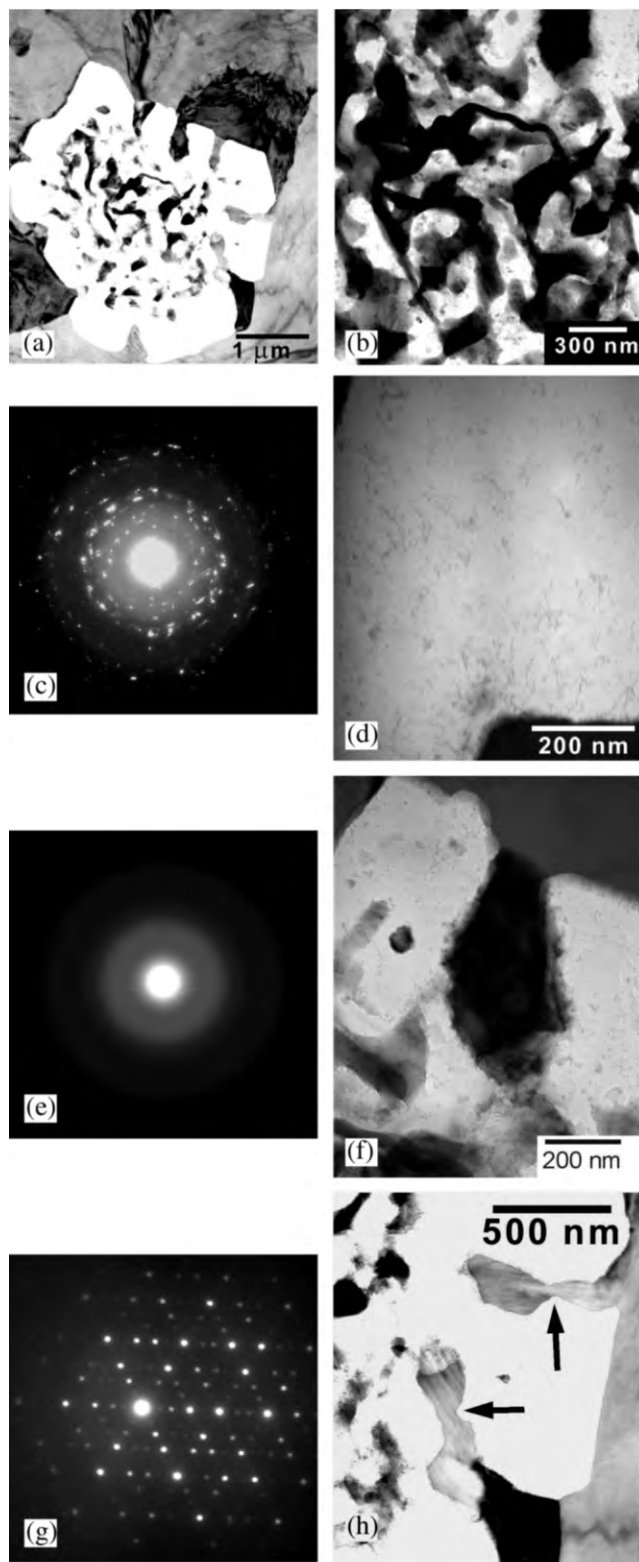


Fig. 5.

High-resolution electron microscopy is required to confirm this hypothesis. Fig. 3e shows the diffraction pattern along 213 zone axis of image in Fig. 3a; strong spots correspond to the matrix (β -phase) spots and weaker spots to the secondary phases. It is evident that the secondary phases are highly textured from the non-existence of ring patterns.

For the sample that was further annealed in air at 500 °C after annealing at 400 °C in Ar, the average composition of the film was $(\text{Al}_{65\pm3}\text{Cu}_{22\pm2}\text{Fe}_{13\pm1})_{84}\text{O}_{16}$. The high oxygen content was attributed to a surface oxide since the thickness of the film was only approximately 150–200 nm. On annealing at higher temperature, the intermetallic grains transformed into icosahedral ψ -grains. This film structure showed a large amount of the ψ -phase with grain sizes on the order of microns, similar to the grain sizes of the crystalline cubic β -phase. Fig. 4a–c show a bright field image of an icosahedral grain oriented along a five-fold axis and the diffraction patterns of icosahedral grains from different zone axes. In some cases, regions which had the external shape that would be expected of a grain, but only contained fragments, were observed as shown in Fig. 5a. We interpret this as a sacrificial grain, which decomposed during the phase transformations on annealing at the higher temperature. Three main features were identified in these regions, namely a mixture of phases of composition $(\text{Al}_{78\pm4}\text{Cu}_{3\pm1}\text{Fe}_{19\pm2})_{75\pm4}\text{O}_{25\pm4}$ that was located within the region (Fig. 5b–c); an amorphous alumina residue with composition $(\text{Al}_{97\pm1}\text{Fe}_{3\pm1})_{42\pm2}\text{O}_{58\pm2}$ (Fig. 5d–e); and an icosahedral grain adjoining the region (Fig. 5f–g).

The existence of the sacrificial grains is attributed to the composition fluctuation from the perfect icosahedral composition. These grains allow others to transform into ψ -phase. It appears that the elements diffuse into neighboring grains without significant migration of grain boundaries. Elements near the boundary of the sacrificial grain diffused into other grains to form the ψ -phases (Fig. 5f) leaving fragments in the center of the grain. Areas where the elements diffused out from the grains (Fig. 5d) were identified as the oxide layer.

The fragments in the center of the grain, with the average composition of $\text{Al}_{78\pm4}\text{Cu}_{3\pm1}\text{Fe}_{19\pm2}$ (excluding the oxygen), have the composition of the λ -phase. Most

Fig. 5. (a) Image of sacrificial grain due to phase transformation into quasicrystalline phases. The three main features associated with the transformation are shown in Fig. 5b–h; (b) TEM image of a mixture of phases remaining in the region; (c) the corresponding diffraction pattern of phases in Fig. 5b; (d) TEM image showing the amorphous alumina residue; (e) the corresponding diffraction pattern of the amorphous alumina residue; (f) TEM image of an icosahedral grain adjoining the sacrificial grain; (g) the corresponding diffraction pattern of the icosahedral grain; (h) formation of λ -phase fragments.

spots in the diffraction pattern in Fig. 5c, can be indexed as the λ -phase, the rest is due to minor secondary phases. The λ -phase is the monoclinic $\text{Al}_{13}\text{Fe}_4$ -phase (with $a=1.5489$ nm, $b=0.80831$ nm, $c=1.2476$ nm and $\beta=107.72^\circ$ [41]), which extends up to 6% atomic percentage of Cu. Similar to the crystalline β -phase that creates secondary phases (θ - and ω -phases) in 400° annealed samples, the ψ -phase expels the excess aluminum element in the form of λ -phase. The mechanism of the λ -phase expulsion can be inferred from Fig. 5h. Excess elements segregate to the grain boundaries with the sacrificial grains creating finger-like shapes. The finger-like shape becomes a fragment due to curvature reduction diffusion (shown by the arrows in Fig. 5h) and coalesces with others to form the mixtures of fragments observed in Fig. 5b. These fragments become interconnected by further diffusion.

We hypothesize that the mass transfer by diffusion of the elements to the neighboring grains is higher than what can be accommodated by lateral grain growth. This leads to a rapid growth along the third dimension, resulting in films with high roughness. Bonasso et al. reported observation of clusters with size of 500–1000-nm wide upon annealing Al–Cu–Fe film of 150-nm thickness [42]. This effect has also been observed in a similar growth of 150 nm Al–Cu–Fe–Cr quasicrystalline thin films where the average roughness was more than 50 nm after phase transformation [35]. The roughening phenomenon is prominent in thin films where the grain size is comparable to or larger than the film thickness.

In a sputter deposition of Al–Cu–Fe film on a heated substrate at 460°C , Eisenhammer and Trampert [30] reported that for coverage equal to 3.5 nm the Al–Cu–Fe icosahedral phase grows as isolated nano-particle with a mean diameter of approximately 15 nm and projected layer thickness amounted to 13–14 nm. Therefore, the high-temperature as-deposited Al–Cu–Fe film in their experiment is discontinuous, similar to our annealed sample at 500°C . Our previous study on Al–Cu–Fe–Cr decagonal thin films shows similar behavior upon annealing at 310°C [35], where the decagonal and the hexagonal approximant coexist with other crystalline phases exhibiting a turtle shell-like pattern with large plateaus surrounded by channels.

In addition to diffusion, the interface and surface energies of the phases also play an important role in the microstructural evolution. The lower surface energy of icosahedral phase compared to the crystalline phases results in a preference to grow as islands. A more accurate theory on the cubic–icosahedral phase transformation, in relationship with morphology and microstructural evolution, requires in-situ heating TEM study where nucleation and phase growth can be observed directly. Nevertheless, we believe our proposed micro-

Microstructural evolution in Al-Cu-Fe quasicrystalline thin films

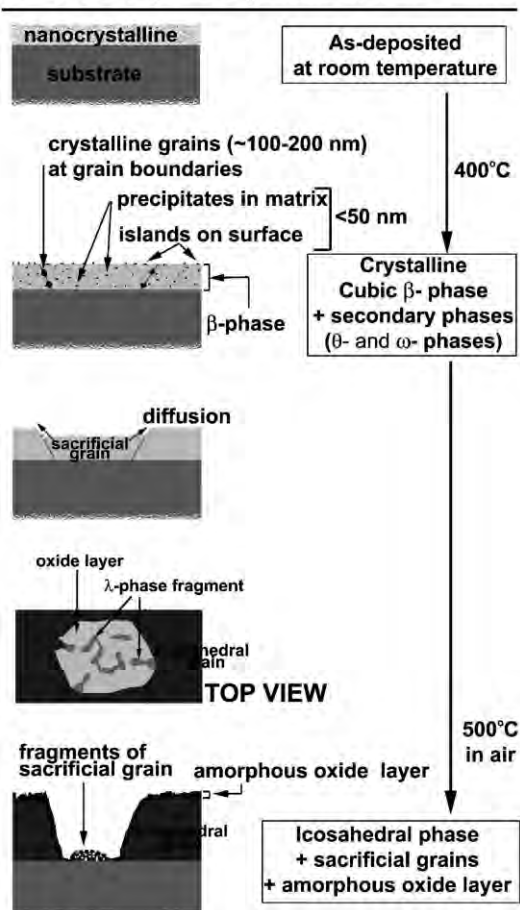


Fig. 6. Schematic of microstructural evolution in Al–Cu–Fe quasicrystalline thin films.

structural evolution in β – ψ -phase transformation, as summarized in Fig. 6, based on our observation to be substantial even though the mechanism is not directly observed.

Furthermore, Fig. 2a and Fig. 4a show that both crystalline and quasicrystalline grains have comparable sizes—on the order of microns. By implementing a two-stage annealing process, the size of the icosahedral grains can be controlled indirectly with a lower temperature anneal prior to phase transformation.

The oxidized regions of the film, which from EDX were identified to be almost pure aluminum oxide, were fairly stable at this annealing temperature. This oxide layer residue was similar to the oxide layer elsewhere on the film, due to oxidation at high temperature (Fig. 7a), and was amorphous (Fig. 7b). This was also observed in Al–Cu–Fe–Cr thin films where annealing at 575°C resulted in a thin residue of aluminum oxide [35]. It was observed that this oxide layer delaminated

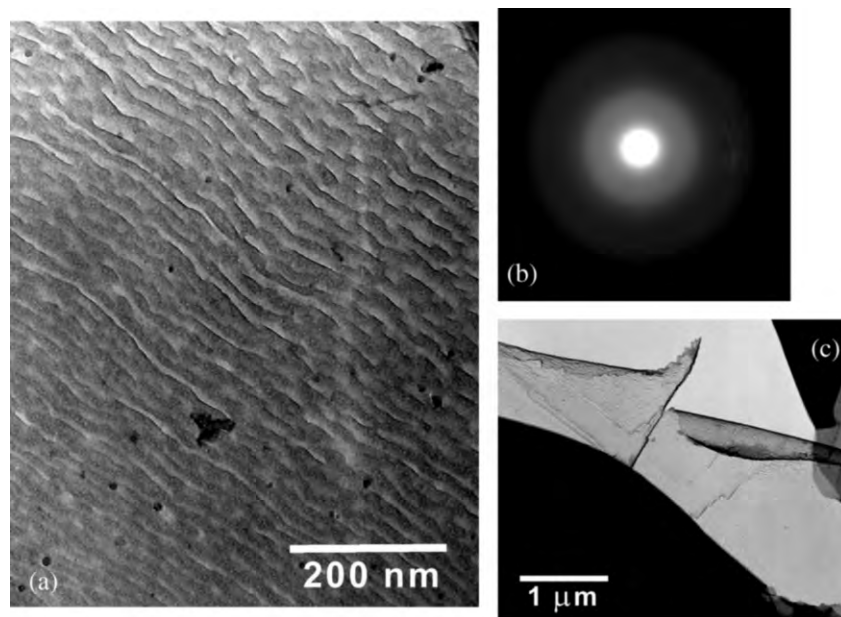


Fig. 7. (a) TEM image of the oxide layer of the film showing an amorphous structure; (b) diffraction pattern of the oxide layer; and (c) delamination of the oxide layer from the quasicrystalline film.

easily, indicating poor adhesion to the quasicrystalline film (Fig. 7c).

4. Conclusions

The as-deposited Al–Cu–Fe thin film has a nanocrystalline structure, which subsequently transformed to micron-size grains of intermetallic phases upon annealing at temperatures below the phase transformation temperature. The cubic β -phase is the dominant phase among the crystalline phases in the sample. The secondary phases (θ - and ω -phases), which appear as small islands and precipitates on surfaces, in matrices and at grain boundaries, were also observed and have textured relationship with the cubic β -phase. At temperatures above the phase transformation temperature, the intermetallics reacted to form icosahedral phases with sacrificial grains. The roles of the sacrificial grains and elemental diffusion and their relationship to microstructural evolution and film morphology were discussed. The oxide layer of the film in the sample annealed at 500 °C in air was amorphous, nearly pure alumina. This aluminum oxide layer had a poor adhesion to the quasicrystalline film.

Acknowledgments

This work was supported by AFOSR-DOD through Grant Award # F49620-96-0214. The authors would like to thank Technology Assessment and Transfer (TA&T) Inc. for providing the sputtering target.

References

- [1] J.M. Dubois, *Mater. Sci. Eng. A* 294 (2000) 4.
- [2] M.F. Besser, T. Eisenhammer, *Mater. Res. Bull.* 22 (1997) 59.
- [3] P. Archambault, C. Janot, *Mater. Res. Bull.* 22 (1997) 48.
- [4] C.J. Jenks, P.A. Thiel, *Mater. Res. Bull.* 22 (1997) 55.
- [5] K. Urban, M. Feuerbacher, M. Wollgarten, *Mater. Res. Bull.* 22 (1997) 65.
- [6] C.J. Jenks, P.A. Thiel, *Langmuir* 14 (1998) 1392.
- [7] A.P. Tsai, A. Inoue, T. Masumoto, *Jpn. J. Appl. Phys.* 26 (1987) L1505.
- [8] M. Quiquandon, A. Quivy, J. Devaud, F. Faudot, S. Lefebvre, M. Bessiere, Y. Calvayrac, *J. Phys.: Condens. Matter* 8 (1996) 2487.
- [9] B. Grushko, R. Wittenberg, D. Holland-Moritz, *J. Mater. Res.* 11 (1996) 2177.
- [10] F.W. Gayle, A.J. Saphiro, F.S. Biancanello, W.J. Boettinger, *Metal. Trans. A* 23A (1992) 2409.
- [11] D. Gratias, Y. Calvayrac, J. Devaud-Rzepski, F. Faudot, M. Harmelin, A. Quivy, P.A. Bancel, *J. Non-Cryst. Solids* 153 (1993) 482.
- [12] A. Kanjilal, U. Tiwari, R. Chatterjee, *Mater. Res. Bull.* 37 (2002) 343.
- [13] M.F. Besser, D.J. Sordelet, in: A.I. Goldman, D.J. Sordelet, P.A. Thiel, J.M. Dubois (Eds.), *New Horizons in Quasicrystals: Research and Applications Conference Proceedings*, World Scientific Singapore, 1997, pp. 288–295.
- [14] R. Teghil, L. D'Alessio, M.A. Simone, M. Zaccagnino, D. Ferro, D.J. Sordelet, *Appl. Surf. Sci.* 168 (2000) 267.
- [15] T. Grenet, F. Giroud, K. Loubet, A. Bergman, G. Safran, J. Labar, P. Barna, J.L. Joulaud, M. Capitan, *J. Alloy Compd.* 342 (2002) 1.
- [16] J. Copola, F. Audebert, S. Duhalde, *Mater. Sci. Forum* 403 (2002) 27.
- [17] N.K. Mukhopadhyay, G.C. Weatherly, *Mater. Sci. Eng. A* 304 (2001) 855.

- [18] M. Takeda, S. Sakai, A. Kawasaki, A.Y. Hattori, M. Katoh, *Mater. Sci. Eng. A* 294 (2000) 842.
- [19] C.I. Lang, D.J. Sordelet, M.F. Besser, D. Shechtman, F.S. Biancaniello, E.J. Gonzales, *J. Mater. Res.* 15 (2000) 1894.
- [20] S.S. Kang, J.M. Dubois, *J. Mater. Res.* 8 (1993) 2471.
- [21] T. Klein, O.G. Symko, C. Paulsen, *Phys. Rev. B.* 51 (1995) 12 805.
- [22] R. Haberkern, K. Khedhri, C. Madel, P. Haussler, *Mater. Sci. Eng. A.* 294 (2000) 475.
- [23] A. Haugeneder, T. Eisenhammer, A. Mahr, J. Schneider, M. Wendel, *Thin Solid Films* 307 (1997) 120.
- [24] T. Grenet, F. Giroud, C. Loubet, J.L. Joulaud, M. Capitan, *Mater. Sci. Eng. A* 294 (2000) 838.
- [25] T. Grenet, F. Giroud, J.L. Joulaud, M. Capitan, *Phil. Mag. A.* 82 (2002) 2909.
- [26] P.A. Bancel, *Philos. Mag. Lett.* 67 (1993) 43.
- [27] P.B. Barna, *Phys. Scr.* T49A (1993) 349.
- [28] I. Levi, D. Shechtman, *J. Mater. Sci.* 27 (1992) 5553.
- [29] E. Emeric, C. Bergman, G. Glugnet, P. Gas, M. Audier, *Philos. Mag. Lett.* 78 (1998) 77.
- [30] T. Eisenhammer, A. Trampert, *Phys. Rev. B* 78 (1997) 262.
- [31] Y. Ding, D.O. Northwood, A.T. Alpas, *Surf. Coat. Technol.* 96 (1997) 140.
- [32] A. Yoshioka, K. Edagawa, K. Kimura, S. Takeuchi, *Jpn. J. Appl. Phys.* 34 (1995) 1606.
- [33] C.L. Chien, M. Lu, *Phys. Rev. B* 45 (1992) 12 793.
- [34] C. Roth, G. Schwalbe, R. Knofler, F. Zavaliche, O. Madel, R. Haberkern, P. Haussler, *J. Non-Cryst. Solids* 252 (1999) 869.
- [35] E.J. Widjaja, L.D. Marks, *Thin Solid Films* 420 (2002) 295.
- [36] M. Ohring, *The Materials Science of Thin Films*, Academic Press Ltd, London, 1992, p. 235.
- [37] Y. Qin, R. Wang, Q. Wang, Y. Zhang, C. Pan, *Philos. Mag. Lett.* 71 (1995) 83.
- [38] X. Yang, R. Wang, X. Fan, *Philos. Mag. Lett.* 73 (1996) 121.
- [39] Z. Shen, M.J. Kramer, C.J. Jenks, A.I. Goldman, T. Lograsso, D. Delaney, M. Heinzig, W. Raberg, P.A. Thiel, *Phys. Rev. B* 58 (1998) 9961.
- [40] F.W. Gayle, *J. Phase Equilib.* 13 (1992) 619.
- [41] P.J. Black, *Acta Cryst.* 8 (1955) 43.
- [42] N. Bonasso, P. Pigeat, D. Rouxel, B. Weber, *Thin Solid Films* 409 (2002) 165.